Development, amplification, and decay of Atlantic/European summer weather patterns linked to spring North Atlantic sea surface temperatures

Article

Accepted Version

Ossó, A., Sutton, R., Shaffrey, L. and Dong, B. (2020) Development, amplification, and decay of Atlantic/European summer weather patterns linked to spring North Atlantic sea surface temperatures. Journal of Climate, 33 (14). pp. 5939-5951. ISSN 1520-0442 doi: https://doi.org/10.1175/jcli-d-19-0613.1 Available at http://centaur.reading.ac.uk/91492/

To link to this article DOI: http://dx.doi.org/10.1175/jcli-d-19-0613.1

Publisher: American Meteorological Society

Development, amplification and decay of Atlantic/European summer weather patterns linked to spring North Atlantic sea surface temperatures

***Albert Ossó*[1,2]*, Rowan Sutton*[2]*, Len Shaffrey*[2] *and Buwen Dong*[2]**

[1] Wegener Center for Climate and Global Change

[2] NCAS-Climate, University of Reading, Reading, United Kingdom

Corresponding author: Albert Ossó. Email address: albert.osso-castillon@uni-graz.at

Abstract

A recent study identified a relationship between North Atlantic SST gradients in spring and a specific pattern of atmospheric circulation in the following summer: the summer East Atlantic (SEA) pattern. It was shown that the SEA pattern is closely associated with meridional shifts in the eddy-driven jet in response to anomalous SST gradients. In this study, the physical mechanisms underlying this relationship are investigated further. It is shown that the predictable SEA pattern anomalies appear in June-July and undergo substantial amplification between July and August before decaying in September. The associated SST anomalies also grow in magnitude and spatial extent from June to August.

The question of why the predictable atmospheric anomalies should occur in summer is addressed, and three factors are identified. First is the climatological position of the storm track, which migrates poleward from spring to summer. Secondly, the magnitude of interannual SST variability underlying the storm track peaks in summer, both in absolute terms, and relative to the underlying mean SST gradient. The third factor is the most interesting. We identify a positive coupled ocean-atmosphere feedback, which operates in summer and leads to the amplification of both SST and atmospheric circulation anomalies.

The extent to which the processes identified are captured in the HadGEM3-GC2 climate model is also assessed. The model is able to capture the relationship between spring

Early Online Release: This preliminary version has been accepted for publication in *Journal of Climate*, may be fully cited, and has been assigned DOI 10.1175/JCLI-D-19-0613.1. The final typeset copyedited article will replace the EOR at the above DOI when it is published.

North Atlantic SSTs and subsequent ocean-atmosphere conditions in early summer, but the relationship is too weak. The results suggest that the real world might be more predictable than inferred from the models.

1. Introduction

The impact of the oceans on the large scale atmospheric circulation has received substantial attention from the climate forecasting community. Two-way air-sea interactions play a key role in tropical variability (e.g., Horel and Wallace 1981; Webster 1998), with the El Niño Southern Oscillation (ENSO) the most prominent example (e.g., Rasmusson and Wallace 1983; Philander 1983). At extratropical latitudes, the coupling between the atmosphere and ocean has generally been considered to be weaker than in the tropics (e.g, Kushnir *et al.* 2002 and references therein). However, new evidence suggests that the impact of the North Atlantic Ocean on the summertime extratropical atmosphere might be more important than previously thought. Gastineau and Frankignoul (2015) used a lagged maximum covariance analysis to investigate possible relations between North Atlantic SSTs and Euro-Atlantic atmospheric circulation. The authors found evidence that a large scale summer Z500 anomaly over the North Atlantic covaries with a precursor spring North Atlantic SST tripole pattern. Duchez *et al.* (2016) also presented evidence linking North Atlantic Sea Surface Temperature anomalies to the occurrence of European heat waves. In more recent work, Ossó *et al.* (2018) show evidence that the SST pattern reported by Gastineau and Frankignould (2015) is forced by anomalous atmospheric circulation during winter and spring, and that it then persists into summer when it influences the position of the jet stream in July-August (JA) by changing the background baroclinicity. The surface fingerprint of this jet displacement features an anomaly in sea level pressure (SLP) over the Northeast Atlantic, with its maximum centred west of the British Isles; the authors refer to this as the Summer East Atlantic (SEA) pattern. Ossó *et al.* 2018 showed that an index of North Atlantic SST in

March-April (MA) can predict the SEA pattern in July-August (JA) with a cross-validated skill of 0.67. The SEA pattern has a strong influence on rainfall over Ireland, the United Kingdom and North Western Europe, and it was shown that summer rainfall in this region can also be predicted with significant skill by a simple statistical model that includes the spring SST index as a predictor.

There is also evidence that summer atmospheric circulation in western Europe is subject to influences from the tropics. Wulff *et al.* 2017 show evidence that the second mode of summer low frequency variability in the Euro-Atlantic region is forced by diabatic heating anomalies, associated with tropical rainfall of opposing signs in the tropical Pacific and Caribbean. Coincidentally the authors described this mode also as the “Summer East Atlantic” (SEA) pattern. However, it is important to note that the SEA mode defined by Wulff *et al.* 2017 is different to that described by Ossó *et al.* 2018. O’Reilly *et al.* 2018 report that the dominant mode obtained from a Maximum Covariance Analysis between the summer Euro-Atlantic circulation and tropical precipitation features a cyclonic anomaly over the extratropical Atlantic, which resembles the Wulff *et al.* 2017 SEA pattern.

Dynamical seasonal forecast of European summer climate have until recently shown very little skill (e.g., Scaife *et al.* 2014; Arribas *et al.* 2011). However, a recent study by Dunstone *et al.* 2018 showed for the first time evidence of skilful dynamical predictions of European summer rainfall obtained using the latest high-resolution Met Office near-term prediction system. The authors show that the skill is linked to predictable North Atlantic SST variability which influences the supply of moisture over Europe and modulates convective rainfall. Despite representing important progress, this model has almost no skill in predicting the circulation variability, indicating that the model skill is primarily linked to thermodynamic processes. The results of Wulff *et al.* 2017, Ossó *et al.* 2018, and O’Reilly *et al.* 2018 therefore suggest that there is significant potential to improve the skill of dynamical seasonal forecasts by improving the fidelity which they can capture predictable dynamical (i.e. circulation) signals. This opportunity motivates the need to better understand the processes that govern these signals, and to assess their representation in forecast models.

The purpose of this paper is to further investigate the predictable signals discussed in Ossó *et al*. 2018. Our primary aim is to identify and quantify the physical mechanisms that govern the intraseasonal evolution - from June to September - of the SEA pattern and its associated SST anomalies. In addition, we include a basic evaluation of the extent to which the mechanisms that operate in the real world are accurately simulated in the HadGEM3-GC2 global climate model used for seasonal forecasting at the UK Met Office.

The paper is organized as follows: Section 2 describes the data and the analysis techniques. In Section 3 we analyse the temporal and spatial evolution of the SEA pattern and associated SST anomalies, and the physical processes involved. In Section 4 we assess the ability of a global climate model (HadGEM3-GC2) to simulate the observed SEA pattern-SST relationship. Conclusions and implications are in Section 5.

2. Data and analysis techniques

We analyse monthly mean data from ECMWF Interim Reanalysis (ERA-Interim) (Dee *et al*. 2001). The analysis is performed on a 2.5° x 2.5° grid for the period 1979-2017 except if indicated otherwise in the figure captions. The regions where sea-ice concentration exceeds 1% are excluded from the SST field before analysis. To test the sensitivity of the results to the dataset used we have repeated the analysis using SLP data from HadSLP2 (Allan and Ansell 2006) and SST data from HadSST3 (Smith *et al*. 2008). The results do not change and all the conclusions stand the same. In Ossó *et al*. 2018 the SEA pattern is analysed using bimonthly mean anomalies. This choice is adequate to study the inter-annual variability of the pattern. Here however we are interested to investigate the intra-seasonal evolution of the SEA pattern during the summer months (from June to September) so monthly means are used instead. The data is linearly detrended to remove the influence of long-term trends. Anomalies are calculated by subtracting the corresponding monthly climatology. In addition to the observational and reanalysis data, model simulation data from a 120 year preindustrial control run with the Met Office Global Coupled model 2.0 (HadGEM3-GC2) (Williams *et al*. 2015) is also analysed.

Ossó *et al*. 2018 identifies a North Atlantic pattern of covariability between SSTs and SLP and show that this pattern can be characterized with an SST index. The North Atlantic SST index (Fig S1) is calculated by averaging the March-April (MA) SST anomalies over the north-western box shown in Fig.1 (42°N–52°N; 52°W–40°W) minus the MA SST anomalies averaged over the south-eastern box (35°N–42°N; 35° W–20°W). The results are not sensitive to small variations in the region used to define the SST index. To be consistent with Ossó et al. 2018 we use MA mean SSTs to build the index. However, calculating the index using only March or April SSTs do not change the results. The SST index is standardized so it has a mean of zero and a standard deviation of one.

Linear regression and correlation analyses are performed to identify lead-lag linear relationships between variables. The statistical significance of the linear regression coefficients and correlations is estimated using a two-tailed Student's t-test with adjusted degrees of freedom to account for the autocorrelation of the time series following the methodology outlined in Santer *et al*. 2001.

The Eady growth rate is used as a measure of local baroclinic instability (Hoskins and Valdes 1990). The Eady growth rate is defined as 0.31(f/N)(du/dz), where f is the Coriolis parameter, N is the Brunt-Väisällä frequency, z is the vertical coordinate and u is the zonal wind. Storm track analysis is based on the tracking scheme developed by Hodges 1995, which identifies extratropical cyclones as 850-hPa relative vorticity maxima using 6 hourly data from the ERA-Interim reanalysis.

The monthly position of the jet core is identified in the 850-hPa monthly-mean wind field as the grid point with the wind speed maxima, identified using finite differencing. The latitude of the JA mean North Atlantic eddy-driven jet is identified in the 850-hPa zonal wind field following a method similar to that used in Woollings *et al*. 2010. First, the bimonthly zonal wind at 850-hPa is zonally averaged between 0°-60° W over the North Atlantic. Then the latitude of the maximum zonal wind between 20°-75°N is identified in the resulting time series. Probability density functions (PDF) of the jet latitude climatology are calculated using a kernel method (Deng *et al.* 2011). Jet latitude PDFs are also calculated for years with MA SST index larger or smaller than plus one standard deviation (+1σ) or minus one standard deviation (-1σ). The statistical significance of SLP and SST composites is tested by boot-strapping with 1000 iterations the SLP and SST timeseries at each grid point.

Ocean mixed-layer temperature tendency is calculated by taking into account the contributions due to surface radiation, surface turbulent fluxes and Ekman transport, using a seasonally and spatially varying mixed-layer depth climatology from the French Research Institute for Exploration of the Sea (De Boyer *et al*. 2004). For more details on the tendency calculations see the methods section of Ossó *et al*. 2018.

3. Observed development, amplification and decay of the ocean and atmospheric anomalies

3.1. Evolution of SLP and SST anomalies

Figure S1 shows the time evolution of the linearly detrended SST Index. During the period considered in this study (1979- 2017) interanual variations dominate the SST Index. A more detailed study of the temporal evolution of the SST Index is shown in the complementary information of Ossó et al. 2018.

We analyse the evolution of ocean and atmospheric anomalies associated with the MA SST index by performing a lagged linear regression analysis between monthly (from June to September) SLP and SST anomalies with the precursor MA SST dipole index (Fig.1). The SST regression coefficients in Figure 1 indicate the evolution of the SST field. In June, they exhibit a dipole pattern that strongly resembles the precursor SST dipole in spring except the anomalies are weaker (compare Ossó et al. 2018, Fig.2). In July and August, the warm SST anomaly east of Newfoundland intensify and expand northeastward. In September and October, the warm anomaly starts to dissipate and by November, the anomaly magnitude is only about a quarter of that in August and the regression coefficients are no longer statistically significant (not shown).

The SLP regression coefficients indicate the evolution of the atmospheric circulation. Note that since the typical persistence time of the extratropical atmosphere is less than 1 month, large and statistically significant SLP regression coefficients in Fig. 1 suggest an atmospheric response to the underlying ocean. In June, a dipolar pattern of SLP anomalies extends across the North Atlantic, with an anticyclonic anomaly located over Western Europe and northeast Atlantic. In July, a stronger anticyclonic anomaly is centred over the central–east Atlantic. In August, this anticyclonic anomaly intensifies further, in terms of both magnitude and correlation with the preceding MA SST index (Fig. S2); its centre of action is also displaced slightly eastward. In September, the anticyclonic anomaly is no longer present and the anomalies are generally weak and not statistically significant.

3.2 Physical mechanisms

Ossó *et al*. 2018 showed that the SEA pattern is the surface fingerprint of North Atlantic jet stream fluctuations forced by changes in baroclinicity associated with the anomalous spring SST gradient. Here we explore the intraseasonal (June to September) jet variations (Fig. 2a, 2c, 2e and 2g) and Eady growth rate anomalies (Fig. 2b, 2d, 2f and 2h) linearly associated with the MA SST index. The regression pattern shows that June is characterized by weak westerly anomalies poleward of the climatological jet and weak easterly anomalies on its equatorward side. Positive and negative Eady growth rate anomalies are also apparent respectively poleward and equatorward of the jet but these are weak and not statistically significant. In July and August, a similar pattern of zonal wind anomalies is apparent but now the anomalies are substantially larger. There are, as well, concurrent strong positive Eady growth rate anomalies (with a size of about 30% the climatological value) poleward of the jet and slightly weaker negative anomalies (about 20% the size of the climatology) on its equatorward side. The Eady growth rate anomalies are forced by the anomalous SST meridional gradient (figure not shown) and are co-located with the jet core anomalies shown in figure 2. This suggests a possible causality from the latter to the former. However, the same jet anomalies might also force secondary Eady growth rate downstream. Finally, in September the pattern of zonal wind and Eady growth rate anomalies reverses; however, the anomalies are weak and not statistically significant.

Another perspective is obtained by examining the North Atlantic storm track itself, i.e. the paths and other characteristics of extratropical cyclones. Figure 3 shows the regression of JA storm track density (Fig.3a) and storm genesis density (Fig.3b) onto the MA SST index. Figure 3a shows – consistent with Fig 2 - that a positive MA SST index is associated with a poleward shift of the summer jet, with a ~30% density increase South-West of Iceland and a ~30% density decrease east of the UK relative to the JA climatology. There are also changes in the genesis density. Fig.3b shows an increase in genesis density south-east of Greenland and East of Iceland, and a decrease west of the British Isles. The genesis density anomaly south-east of Greenland could be associated with increased Greenland Tip Jet events (Moore and Renfrew 2005; Harden et al. 2011; Harden and Renfrew 2012) due to the favourable conditions associated with the northward displaced jet.

Why should the atmospheric response to the underlying SST – involving the storm track and eddy-driven jet – be strongest in July and August?

Ossó *et al*. 2018 hypothesised that the timing of the atmospheric response may be partly a consequence of the seasonal migration of the North Atlantic eddy driven jet. Here we present evidence that both the seasonal migration of the jet *and* the seasonal evolution of the SST variability contribute to explaining why the atmosphere responds primarily during the summer months.

Figure 4 shows the seasonal variation of the eddy-driven jet latitude (see section 2). In spring the jet is located south of the anomalous SST gradient measured by our SST index, but in summer (from June to September) the jet is located over the region where significant fluctuations in the SST gradient arise. These SST fluctuations are associated with fluctuations in the Eady growth rate as shown in Figure 2 (d and f). Further insight is provided by Figure 5, which illustrates the seasonal variation in both the mean (i.e. climatological) and anomalous (due to interannual variability) SST gradient in the region measured by our index. Fig.5a shows that the climatological SST gradient in this region declines rapidly in July and August, whilst Fig.5b shows that the standard deviation is maximum in the same summer months. Thus the ratio of these two quantities (i.e. standard deviation divided by mean SST gradient index), shown in Fig.5c, shows a very strong peak in July and August. Based on these results we hypothesise that the storm track may be particularly sensitive to variations in the underlying SST gradient, which are about 15% of its mean value.

Overall our findings so far suggest two reasons for a strong atmospheric response in summer:

(i) The storm track is located further north (Fig 4) in a region where there is significant interannual SST variability;

(ii) The magnitude of interannual SST variability in this region peaks in summer, both in absolute terms (Fig 5b) and relative to the underlying mean SST gradient (Fig 5c), which is weaker in summer (Fig 5a).

3.3 Amplification by ocean-atmosphere coupling

Figure 5b shows that the variance of the SST index increases in summer, and Figs 1 and S2 show that this increase does not simply reflect additional uncorrelated summer variance (“noise”) but rather that the magnitude, spatial extent and correlation of the SST variability that is correlated with the MA SST index also increases from June to July and July to August. This finding is surprising, as one would normally expect correlation in particular to decline with lead time. Ossó *et al*. 2018 suggested that this interesting behaviour might be explained by the existence of a positive ocean-atmosphere feedback which amplifies SST and SLP anomalies during the summer months. Here we investigate this hypothesis further.

Figure 6 analyzes the physical processes driving the evolution of the SST anomalies during June-September associated with the MA SST index. Figure 6a, 6d and 6g show the month-to-month change of the SST anomalies; Figure 6b, 6e and 6h show the total mixed layer temperature tendency and Figure 6c, 6f and 6i show the mixed layer temperature tendency due to radiation alone. Note that all three fields are regressed onto the MA SST index. SSTs in the central North Atlantic warm from June to July and from July to August. Detailed examination of the individual processes contributing to the mixed layer temperature tendency (see section 2) shows that the warming is forced by enhanced surface radiation and turbulent fluxes, while anomalous Ekman transports play a minor role. The contribution from increased surface radiation is particularly important for the warming between July and August (Fig 6f) and is associated with a reduction in cloud cover (not shown). The surface flux anomalies implied by Fig 6 arise in response to surface winds and cloud conditions associated with the anticyclonic SEA pattern anomalies shown in Fig 1. But we have already seen that the circulation anomalies themselves amplify, particularly between July and August. Thus our findings support the hypothesis of Ossó *et al*. 2018 that there is a positive coupled ocean-atmosphere feedback that operates over the North Atlantic Ocean in summer time, and provide further insight into the mechanisms involved: SST anomalies east of Newfoundland excite a circulation response which leads to amplification and eastward spread of the SST anomalies, and we hypothesise that also leads to concurrent amplification of the atmospheric circulation anomalies. Note however, that the causality of this last step, the concurrent amplification of the atmospheric anomalies, cannot be inferred from statistical analysis alone since there is no lag between ‘concurrent’ anomalies. Further analysis (e.g. model experiments) may be required to full identify all the steps in the positive feedback. The SST anomalies grow primarily through the influence of turbulent and radiative surface heat fluxes that directly associated with the anomalous atmospheric circulation. The role played by surface radiation and associated cloud changes is especially interesting since it represents a distinctive characteristic of summer mid-latitude air-sea interactions. This coupled ocean-atmosphere amplification is an important additional reason for the strong atmospheric response in summer.

From August to September the SST anomalies cool (Fig 6g) as the atmospheric circulation anomalies also dissipate (Fig 1d). Analysis of the terms contributing to the mixed layer temperature tendency shows that the cooling is largely dominated by anomalous turbulent heat loss associated with the strengthening of the westerlies at around 45° latitude from August to September (Figs 6 h and i).

3.4 Evidence of nonlinearities

So far we have analyzed the linear relationship between the atmosphere circulation and the spring SST gradient. In this section we investigate whether there is evidence for any nonlinear aspects to this relationship. Figure 7a compares the Kernel density distribution of the eddy-driven jet latitude climatology (Woollings et al. 2010) with the distribution for years with large positive and negative values of MA SST index (> +1σ and <-1σ respectively). For positive values of the MA SST index the jet distribution is clearly skewed poleward compared with the climatology while for negative values the distribution is only slightly displaced equatorward. The asymmetry between these distributions does indeed suggest a nonlinear jet response to the MA SST index. We have repeat the analysis of figure 7 using daily zonal wind data instead of bimonthly means (figure not shown). The distributions are very similar and the qualitative results do not change. Further insights can be obtained from a composite of U850 anomalies (Fig.7c and 7d). The U850 anomalies for years with positive values of MA SST index are substantially larger than for years with negative values, again suggesting a nonlinear jet response to the SST anomalies.

Evidence suggests that the nonlinear character of the atmospheric anomalies may result from asymmetries in the SST dipole forcing in July. Figure 8 shows July composites of SSTs (Fig. 8a and 8b), cloud cover (Fig. 8c and 8d) and radiation flux anomalies (Fig. 8e and 8f). Comparison of Figs 8a and 8b shows that large positive values of the MA SST index (> +1σ) are associated with a much clearer dipole pattern than is the case for negative values of the index. However, there is also a role for changes in cloud cover and surface radiation, as shown by Figs 8c and e. Changes in cloud cover and surface radiation also occur in association with large negative values of the MA SST index (Figs 8d and f), but these changes are noisier over the subtropical region than is the case for positive values of the SST index.

Overall the evidence is that large positive values of the MA SST index excite the strongest atmosphere-ocean response in summer.

4. Representation of the SEA pattern - spring SST relationship in HadGEM3-GC2

The evidence from Osso et al 2018 and Section 3 of this paper suggests that the relationship between spring North Atlantic SST anomalies and the summer atmospheric circulation is an important source of predictability for European summer climate. It is therefore important to assess whether this relationship is captured in climate models used for seasonal forecasting. Here, we analyze the representation of this relationship in a 120-year long control simulation from the Met Office HadGEM3-GC2 model, which has an atmosphere horizontal resolution of N216 (about 60km at midlatitudes) and an ocean resolution of 0.25° (Williams et al. 2015). We start by performing a MCA between the MA mean SSTs and the JA mean SLP of the model (Fig.S3). Figure S3 shows a pattern of SST anomalies in MA that covaries significantly with an SEA-like SLP anomaly in the subsequent JA. The spatial pattern of SST and SLP anomalies is very similar to that obtained by applying MCA to observational data (see Ossó et al. 2018, c.f., Fig.S1). Figure 9 shows the regression patterns of SST and SLP anomalies onto an index representative of the HadGEM3-GC2 MA SST dipole. U850 anomalies are shown in Fig.10. (Note that using an SST index defined as for the observations does not change these results significantly.)

SLP and U850 anomalies for July are consistent with a statistically significant atmosphere response to MA SSTs. The spatial patterns of SLP and SST anomalies are very similar to that seen in observations but the magnitude of anomalies is about half. In August, the contrast is much greater. The SLP anomalies are not statistically significant and the U850 anomalies are barely so. The SST anomalies are also very weak. Whereas in the observations we saw a rapid amplification of the ocean and atmosphere anomalies, in the HadGEM3-GC2 model the anomalies decay. This evidence suggests that HadGEM3-GC2 is able to capture the relationship between spring North Atlantic SSTs and subsequent ocean-atmosphere conditions in early summer, but the relationship is weaker than is observed and the model fails to simulate the positive feedback mechanisms that lead to rapid amplification of the signal between July and August. These findings highlight important opportunities for improving the HadGEM3-GC2 model, with a strong expectation that such improvements would be beneficial for summer seasonal forecasts.

5. Conclusions and implications

In this study we have investigated the physical mechanisms that underpin the relationship identified in Ossó et al. 2018 between a dipolar pattern of spring (March-April, MA) North Atlantic SST anomalies and anomalous atmospheric circulation (particularly associated with the SEA pattern) in the subsequent summer. We have examined the development, amplification and decay of the SST and atmospheric anomalies, with a particular focus on ocean-atmosphere interactions. Key findings are as follows:

- Ossó *et al*. 2018 identified a predictable July-August pattern of atmospheric circulation in the North Atlantic (the SEA, Summer East Atlantic pattern) . More detailed analysis in this study has shown that these anomalies appear in June-July and undergo substantial amplification between July and August before decaying in September. The associated SST anomalies also grow in magnitude and spatial extent from June to July and July to August.
- Monthly analysis further supports the evidence presented by Ossó *et al*. 2018 that the SEA pattern response is a consequence of meridional shifts in the summer storm track and associated eddy-driven jet in response to the SST anomalies. These shifts are closely associated with changes in the Eady growth rate and the underlying meridional SST gradient.
- There are also changes in the storm track genesis density associated with the SST gradient. In particular, the reduction of the genesis density over the Southern SST index box is consistent with the observed poleward displacement of the storm track.
- An important question is why should the predictable atmospheric anomalies occur in summer (specifically July-August)? We have identified three factors:
    (i) In comparison to spring, the storm track and associated eddy-driven jet are located further north in a region where there is significant interannual SST variability.
    (ii) The magnitude of interannual SST variability in this region peaks in summer, both in absolute terms, and relative to the underlying mean SST gradient, which in summer is weak.

(iii) As hypothesized by Ossó *et al*. 2018, a positive coupled ocean-atmosphere feedback operates in summer, which leads to the amplification of both SST and atmospheric circulation anomalies, and is particularly effective between July and August. Amplification of the SST anomalies is caused primarily by anomalous surface turbulent and radiative fluxes; the latter are associated with changes in cloud cover. The enhanced SST anomalies increase the anomalous baroclinicity and thereby excite a stronger atmospheric response. This positive ocean-atmosphere feedback sustains and amplifies the SEA pattern in July and August.

- The SST and SEA pattern anomalies decay in September. The SST anomalies are damped by turbulent surface fluxes.
- There is evidence that the summer atmospheric response to SST anomalies is nonlinear. Large positive values of the MA SST index excite the strongest atmosphere-ocean response in summer. The summer atmospheric response is characterised by a substantial poleward shift in the North Atlantic eddy-driven jet. The associated summer SST anomalies feature positive anomalies across the mid-latitude anomalies extending east from Newfoundland, with negative anomalies in the eastern subtropical Atlantic.
- A global climate model, HadGEM3-GC2, is able to capture the relationship between spring North Atlantic SSTs and subsequent ocean-atmosphere conditions in early summer, but the relationship is weaker than is observed and the model fails to simulate the positive feedback mechanisms that lead to rapid amplification of the signal between July and August.

Recent research on the potential drivers of summer Euro-Atlantic climate suggests that the predictable component of summer atmospheric circulation at seasonal timescales may be larger than previously thought. As discussed in the Introduction, both tropical precipitation [e.g., Wulff *et al*. 2017, O'Reilly *et al*. 2018] and extratropical SST gradients

[Gastineau and Frankingnoul 2015, Duchez *et al.* 2016, Ossó *et al*. 2018 and this study] have shown potential as predictors of the summer Euro-Atlantic climate. Furthermore, recent work by Dunstone *et al*. 2018 shows evidence of skillful seasonal forecasts of summer rainfall over Europe using the latest high-resolution Met Office seasonal prediction system. However, the skill of these predictions is primarily linked to thermodynamic processes - there is insignificant skill for atmospheric circulation - and the magnitude of the predicted signals is much smaller than in the real world. These features are a manifestation of the so-called “signal-to-noise paradox” (Scaife and Smith 2018) which was first identified in seasonal forecasts for European winters (Scaife *et al*. 2014). In this study, we have shown that a key physical process shaping the predictability of Atlantic/European summers - amplification through coupled ocean-atmosphere feedback - is not well represented in the HadGEM3-GC2 model (which is very similar to the model used for seasonal predictions by Dunstone *et al*. 2018). This implies that this weakness could be an important factor in accounting for the signal-to-noise paradox in summer seasonal forecasts (Dunstone *et al*. 2018). Investigating the reasons for the model weaknesses in this regard – for example whether they are due to poor representation of SST-cloud-radiation feedbacks or other processes – will be an important area for future work. It will also be important to evaluate other climate models, especially those used for seasonal predictions, to assess the extent to which the mechanisms we have identified are accurately simulated.

Acknowledgements: This work was supported by SummerTIME project funded through the Natural Environment Research Council (NERC) “Drivers of variability in atmospheric circulation” programme. AO, LS, BD and RS are supported by the U.K. National Centre for Atmospheric Science (NCAS) at the University of Reading.

References

Allan, R., and T. Ansell, 2006: A new globally complete monthly historical gridded mean sea level pressure dataset (HadSLP2): 1850–2004, *J. Climate*, **19**, 5816 – 5842.

Arribas A, *et al.*, 2011: The GloSea4 ensemble prediction system for seasonal forecasting, *Mon. Wea. Rev.* **139**, 1891–1910.

Dee, D. P., S.M. Uppala, A. J. Simmons, P. Berrisford, P. Poli, S. Kobayashi, ... &P. Bechtold, 2011: The ERA-Interim reanalysis: Configuration and performance of the data assimilation system, *Q. J. R. Meteorol. Soc*, **137**, 553 – 597.

Deng, H., H. Wickham, 2011: Density estimation in R. Electronic publication.

Duchez, A., et al., 2016: Drivers of exceptionally cold North Atlantic Ocean temperatures and their link to the 2015 European heat wave. *Environmental Research Letters* 11.7: 074004.

Dunstone, N., D. Smith, A. Scaife, L. Hermanson, D. Fereday, C. O'Reilly, *et al.*, 2018: Skilful seasonal predictions of summer European rainfall, *Geophys. Res. Lett.*, **45**, 3246–3254. https://doi.org/10.1002/2017GL076337.

Gastineau, G., and C. Frankignoul, 2015: Influence of the North Atlantic SST variability on the atmospheric circulation during the twentieth century, *J. Climate*, **28**, 1396 – 1416.

Harden, B. E., I. A. Renfrew, and G. N. Petersen, 2011: A Climatology of Wintertime Barrier Winds off Southeast Greenland. J. Climate, 24, 4701-4717.

Harden, B. E., and I. A Renfrew, 2012: On the Spatial Distribution of high winds of southeast Greenland. Geophysical Reseach Letters, 39, L14806.

Haylock MR, *et al.*, 2008: A European daily high-resolution gridded data set of surface temperature and precipitation for 1950–2006, *J. Geophys Res. Atmos*, **113,** D20119.

Hodges, K. I., 1995: Feature tracking on the unit sphere, *Mon. Wea. Rev*, **123** (12), 3458 – 3465.

Horel, J.D., and J.M. Wallace, 1981: Planetary-Scale Atmospheric Phenomena Associated with the Southern Oscillation, *Mon. Wea. Rev*, **109**, 813 – 829.

Hoskins, B. J., and P.J. Valdes, 1990: On the existence of storm-tracks, *J. Atmos Sci*, **47** (15), 1854 – 1864.

Kushnir, Y., W.A. Robinson, I. Bladé, N.M.J Hall, S. Peng and R. Sutton, 2002: Atmospheric GCM response to extratropical SST anomalies: Synthesis and evaluation, *J. Climate*, **15** (16), 2233 – 2256.

Marshall, J., Y. Kushnir, D. Battisti, P.Chang, A. Czaja, R. Dickson, ... and M. Visbeck, 2001: North Atlantic climate variability: phenomena, impacts and mechanisms, *Int. J. Clim.*, **21** (15), 1863 – 1898.

Moore, G. W. K. and I. A. Renfrew, 2005: Tip jets and barrier winds: A QuikSCAT climatology of high wind speed events around Greenland, J. Climate, 18, 3713-3725.

Rogers, J. C., 1997: North Atlantic storm track variability and its association to the North Atlantic Oscillation and climate variability of northern Europe, *J. Climate*,**10** (7), 1635 – 1647.

Scaife AA, *et al.*, 2014: Skillful long-range prediction of European and North American winters, *Geophys. Res. Lett.,* **41**, 2514–2519.

O'Reilly, C. H., J. Heatley, D. MacLeod, A. Weisheimer, T. N. Palmer, N. Schaller, and T. Woollings 2017: Variability in seasonal forecast skill of Northern Hemisphere winters over the twentieth century, Geophys. Res. Lett., 44, 5729–5738, doi:10.1002/2017GL073736.

O'Reilly, C.H., T. Woollings, L. Zanna, and A. Weisheimer, 2018: The Impact of Tropical Precipitation on Summertime Euro-Atlantic Circulation via a Circumglobal Wave Train, *J. Climate,* **31**, 6481 – 6504, https://doi.org/10.1175/JCLI-D-17-0451.1.

Ossó, A., R. Sutton, L. Shaffrey and B. Dong, 2018: Observational evidence of European summer weather patterns predictable from spring, *PNAS,* **115** (1), 59 – 63.

Philander, S. G. H., 1983: El Nino southern oscillation phenomena, *Nature*, **302** (5906), 295.

Rasmusson, E. M., and J.M. Wallace, 1983:. Meteorological aspects of the El Nino/southern oscillation, *Science*, **222**(4629), 1195 – 1202.

Santer B.D., T.M.L. Wigley, J.S. Boyle, D.J. Gaffen, J.J. Hnilo, D. Nychka, D.E. Parker and K.E. Taylor, 2000: Statistical significance of trends and trend differences in layer-average atmospheric temperature time series, *J. Geophys. Res. Atmos.,* **105,** 7337 – 7356.

Smith, T. M., R.W. Reynolds, T.C. Peterson, and J. Lawrimore, 2008: Improvements to NOAA's historical merged land–ocean surface temperature analysis (1880–2006), *J. Climate*, **21**(10), 2283 –2296.

Scaife, A. A. et al. (2014): Skilful long range prediction of European and North American winters. Geophys. Res. Lett. 41, 2514–2519.

Scaife, A. A. and D. Smith, 2018: A signal-to-noise paradox in climate science. *npj Climate Atmos. Sci.*, 1, http://dx.doi.org/10.1038/s41612-018-0038-4.

Webster, P. J., V. O Magana, T. N. Palmer, J. Shukla, R.A. Tomas, M. U. Yanai and T. Yasunari, 1998: Monsoons: Processes, predictability, and the prospects for prediction, *J. Geophys. Res. Oce.*,**103** (C7), 14451 – 14510.

Williams, K. D., C. M. Harris, A. Bodas-Salcedo, J. Camp, R.E. Comer, D. Copsey, ... and P. Hyder, 2015: The met office global coupled model 2.0 (GC2) configuration, *Geos. Mod. Develop.*, **8**(5), 1509.

Wills S.M., D.W.J. Thompson and L.M. Ciasto, 2016: On the Observed Relationships between Variability in Gulf Stream Sea Surface Temperatures and the Atmospheric Circulation in the North Atlantic, *J. Climate,* **29,** 3719 – 3730.

Woollings, T., A. Hannachi and B. Hoskins, 2010: Variability of the North Atlantic eddy-driven jet stream, *Q. J. R. Meteorol. Soc.*, **136**(649), 856-868.

Wulff, C. O., R.J. Greatbatch, D.I.V. Domeisen, G. Gollan, and F. Hansen, 2017: Tropical Forcing of the Summer East Atlantic Pattern, *Geophys. Res. Lett*, **115**(8), 1083 – 8.

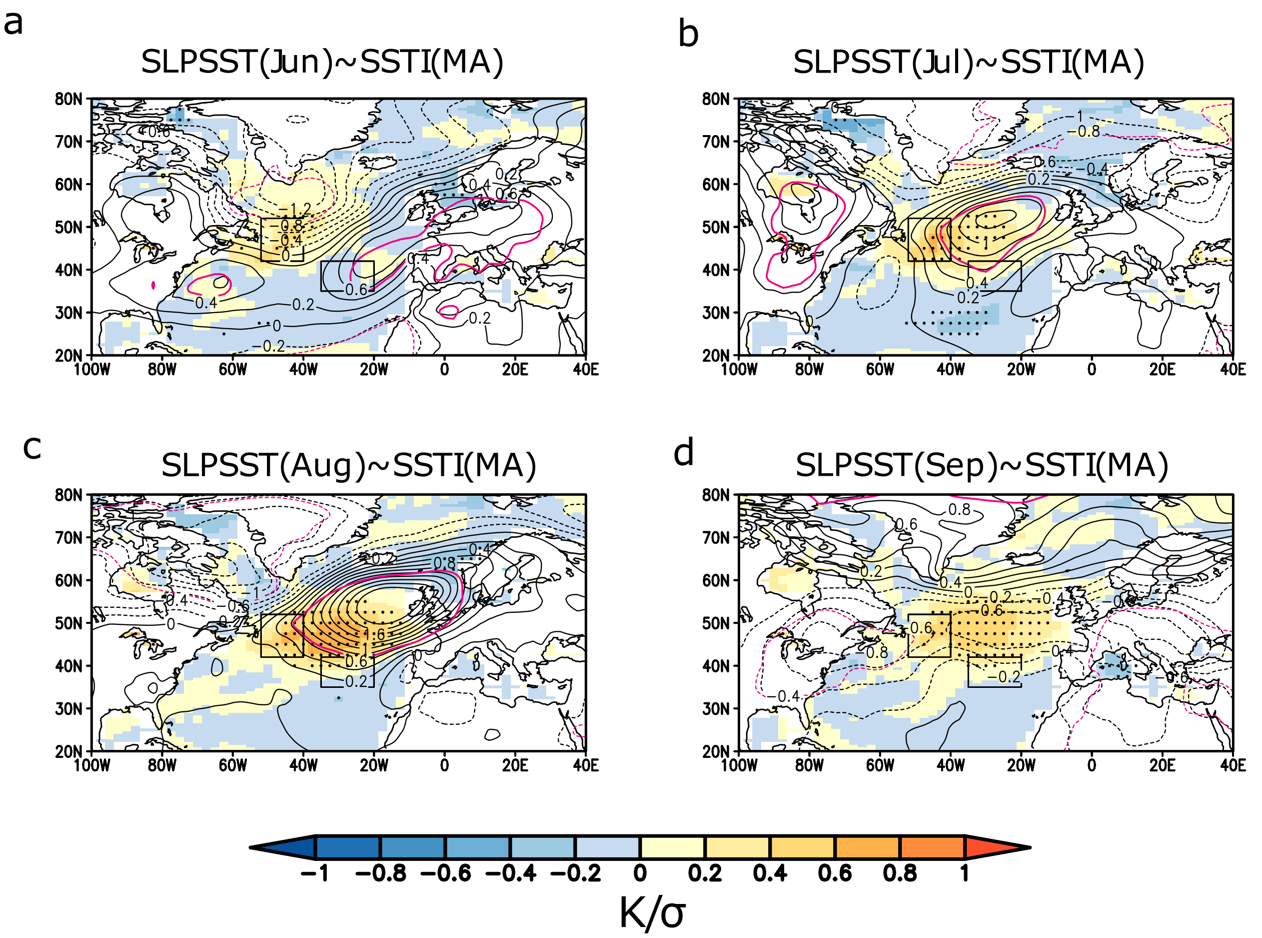

Fig. 1. (a-d) Linear regression maps of the indicated monthly SST (shading) and SLP (contours) anomalies against the precursor MA SST index in ERA-Interim (1979-2017). The SST index is normalized thus the SST and SLP anomalies shown correspond to a standard deviation of the SST index time series. Contour interval is 0.2 hPa σ^{-1}. Stippling indicates SST regression coefficients statistically significant at the 95% confidence level (see section 2). The red contour indicates the critical correlation value between SLP anomalies and the SST index at the 95% confidence level (see section 2). The black boxes indicate the regions used for the SST index, which is calculated as the SST average of the northern box minus the SST average of the southern box.

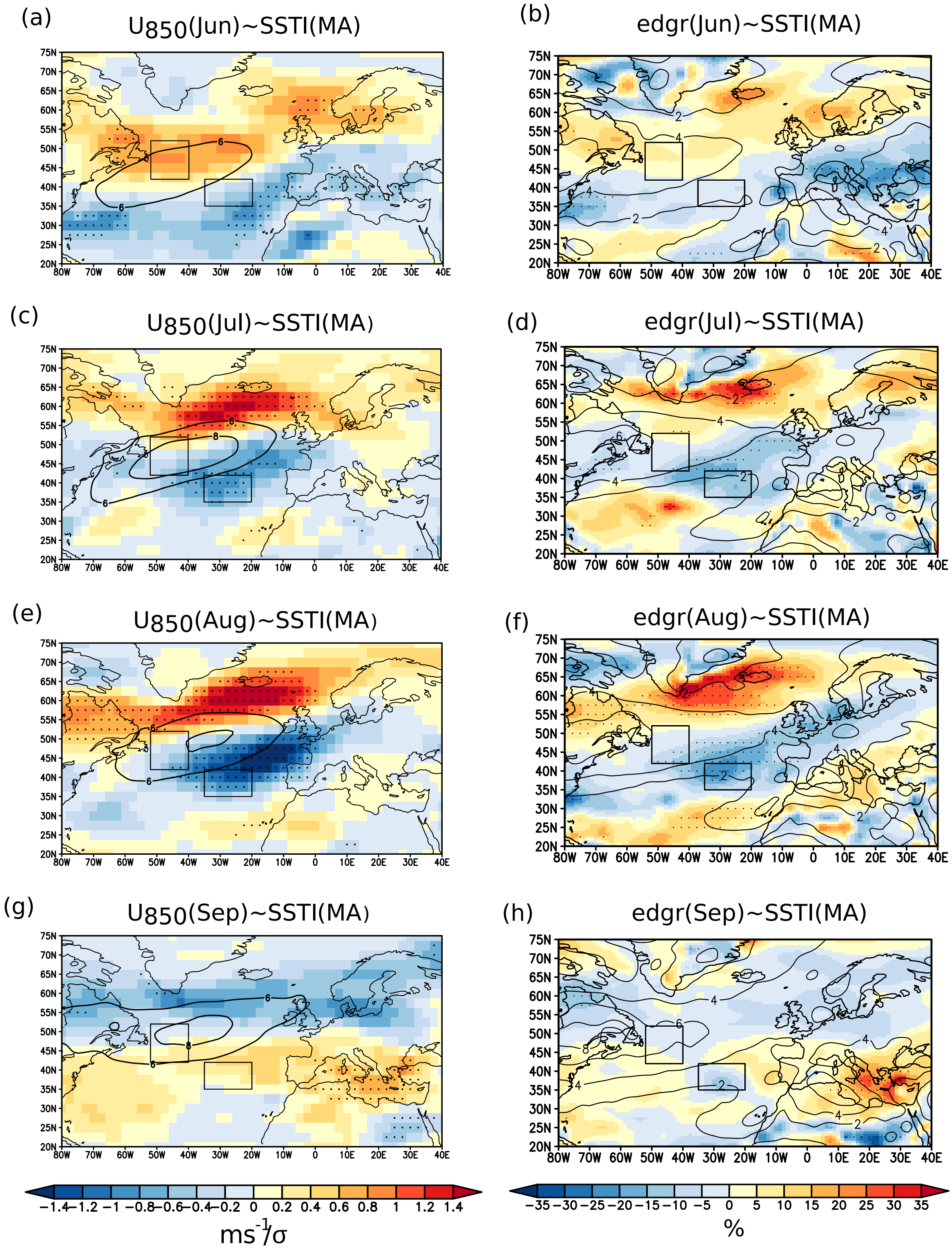

Fig.2 Left column: Linear regression maps of the indicated monthly U_{850} against the precursor MA SST index (shading). The SST index is normalized thus the zonal wind anomalies shown correspond to a standard deviation of the SST index time series. Contours show the corresponding U_{850} climatology (only the largest values are plotted). Stippling indicates U_{850} regression coefficients statistically significant at the 95% confidence level (see section 2). Right column: As in left column, except for eady growth rate (see section 2). The anomalies are expressed as a percentange of its local climatological value. Countours show the corresponding eady growth rate climatology (units: s^{-1} x10^6).

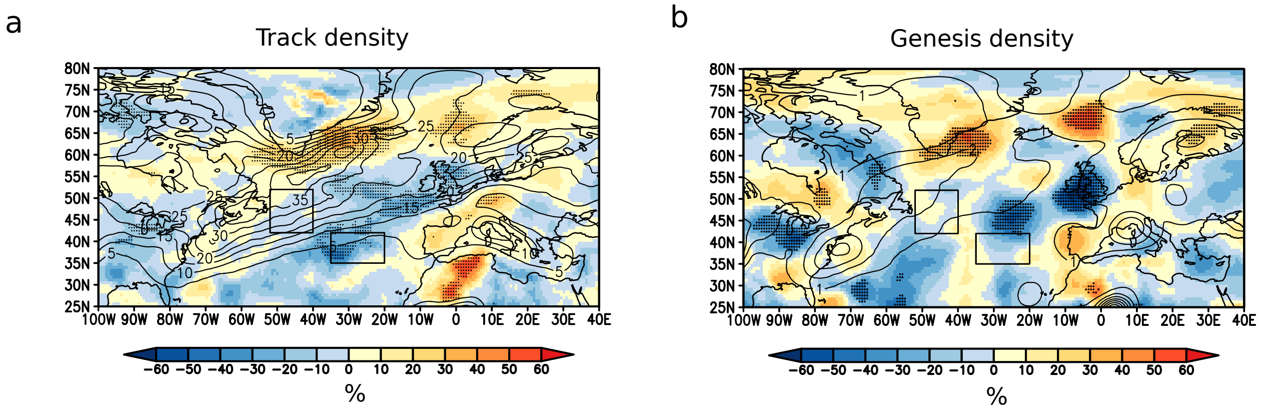

Fig.3 a) Linear regression maps of JA storm track density (a) and genesis density (b) against the MA SST index. The anomaly field is expressed as a percentatge of its local climatological value. Black contours in (a) and (b) are the climatology. Densities are in units of number density per month per unit area, where the unit area is equivalent to a 5° spherical cap ($\sim 10^6$ km^2) (see section 2).

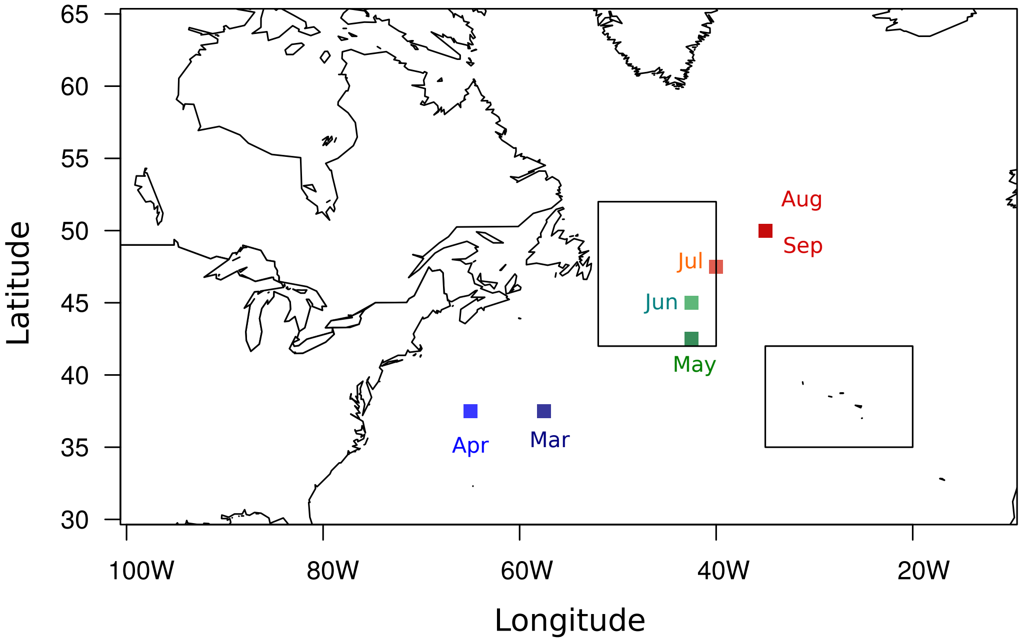

Fig. 4. Seasonal evolution of the geographical position of the North Atlantic eddy-driven jet intensity maximum (see section 2) from March to September.

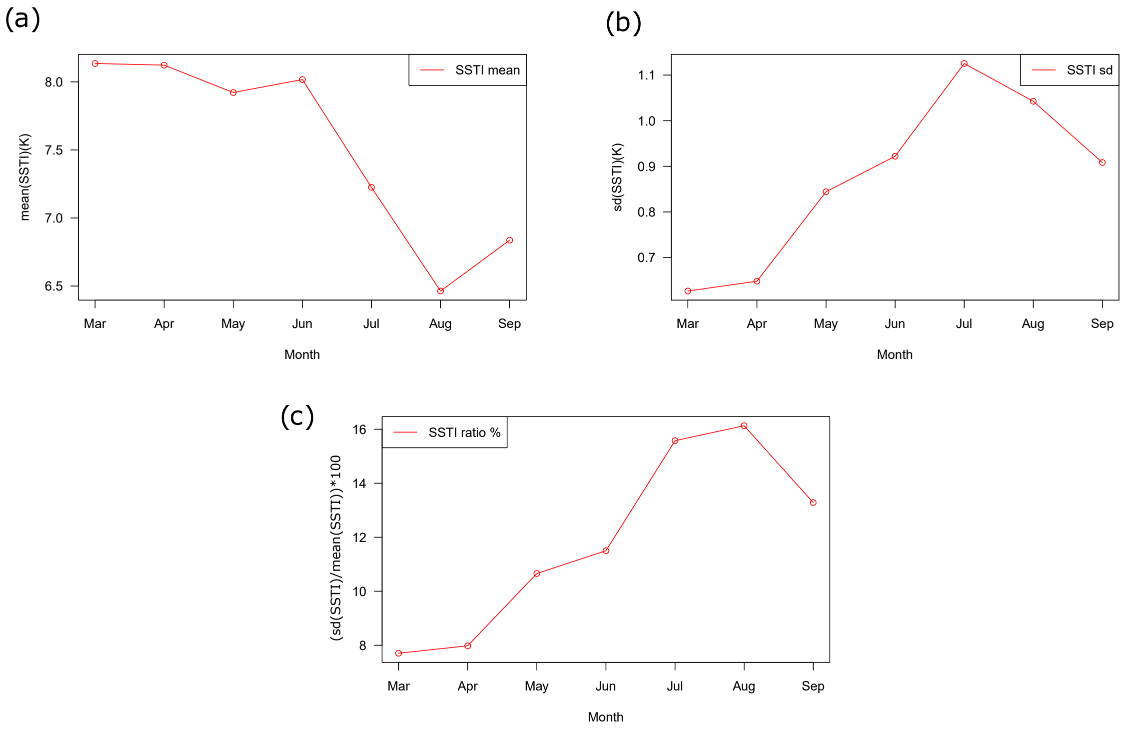

Fig. 5. Seasonal evolution of the monthly SST index (as absolut value (K)) (a), the SST index standard deviation (K) (b) and the ratio between (b) and (a) expressed as a percentatge.

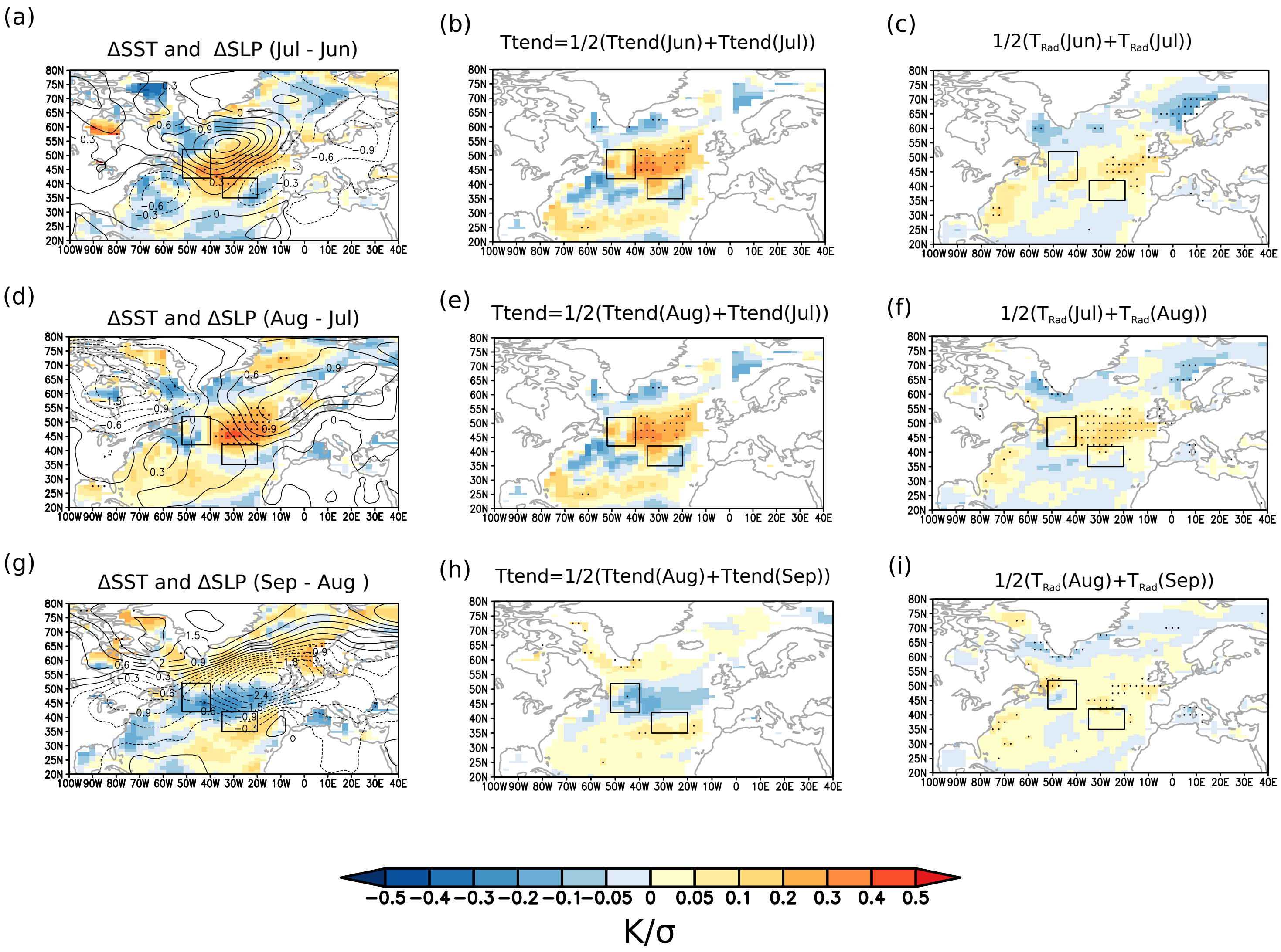

Fig. 6 (a,d,g) Linear regression maps of the SST (shading) and SLP (contours) difference between the months indicated against the MASST index. Contour interval is 0.3 hPa σ^{-1}. (b,e,h) Linear regression maps of the mixed layer ocean temperature tendency (see section 2) for the months indicated against the MA SST index. (c,f,i) As in (b,e,h) but for the temperature tendency due to radiation alone. The MA SST index is normalized thus the anomalies shown correspond to one standard deviation of the MA SST index. Stippling indicates regression coefficients statistically significant at the 95% confidence level (See section 2). The black box indicates the region used to calculate the SST index.

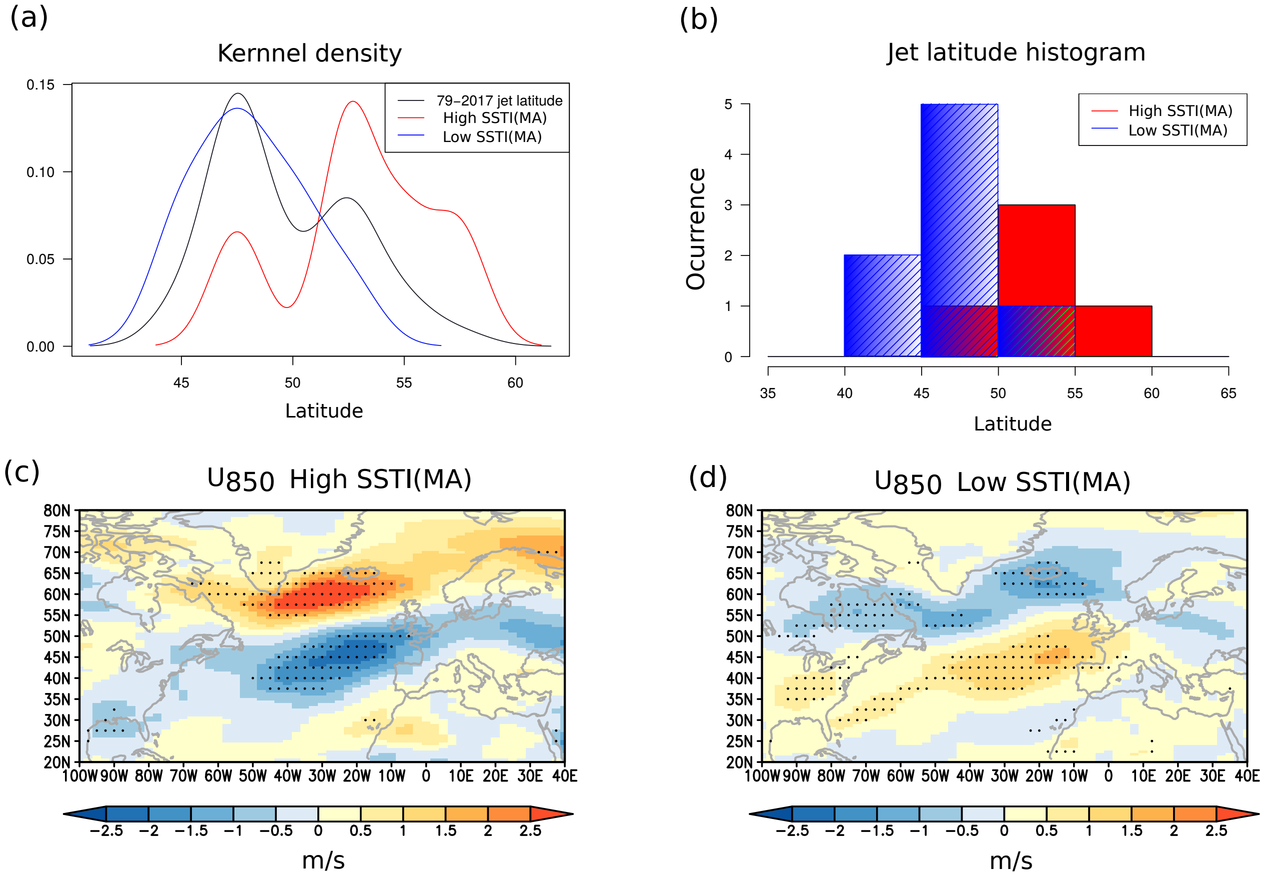

Figure 7: (a) Kernel estimates of the PDF of JA North Atlantic eddy-driven jet latitude in ERA-Interim for the 1979-2017 period (black) and for years with high (red) a low (blue) values of the MA SST Index (See section 2). (b) Distribution of the JA jet stream latitude for high (red) and low (blue) values of the MA SSTI. (c.d) Composites of JA mean U_{850} anomalies for years with high (c) and low (d) values of the MA SSTI. Stippling indicates regions where the composite anomalies are significant at the 95% level estimated using a Monte Carlo resampling method (See section 2).

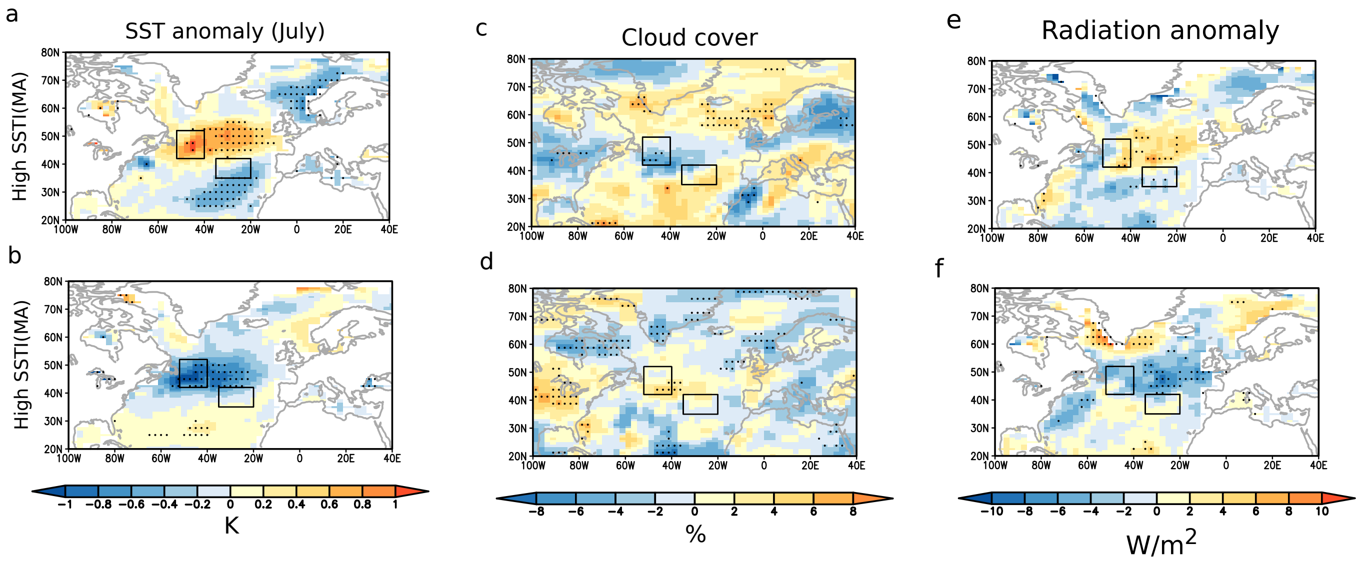

Fig. 8. Upper row: Composites of July SST anomalies (a), cloud fraction (c) and radiation flux (e) for high values of MA SSTI. Bottom row: Same as in upper row except for low values of MA SSTI. Stippling indicates regions where the composite anomalies are significant at the 95% level estimated using a Monte Carlo resampling method (See section 2).

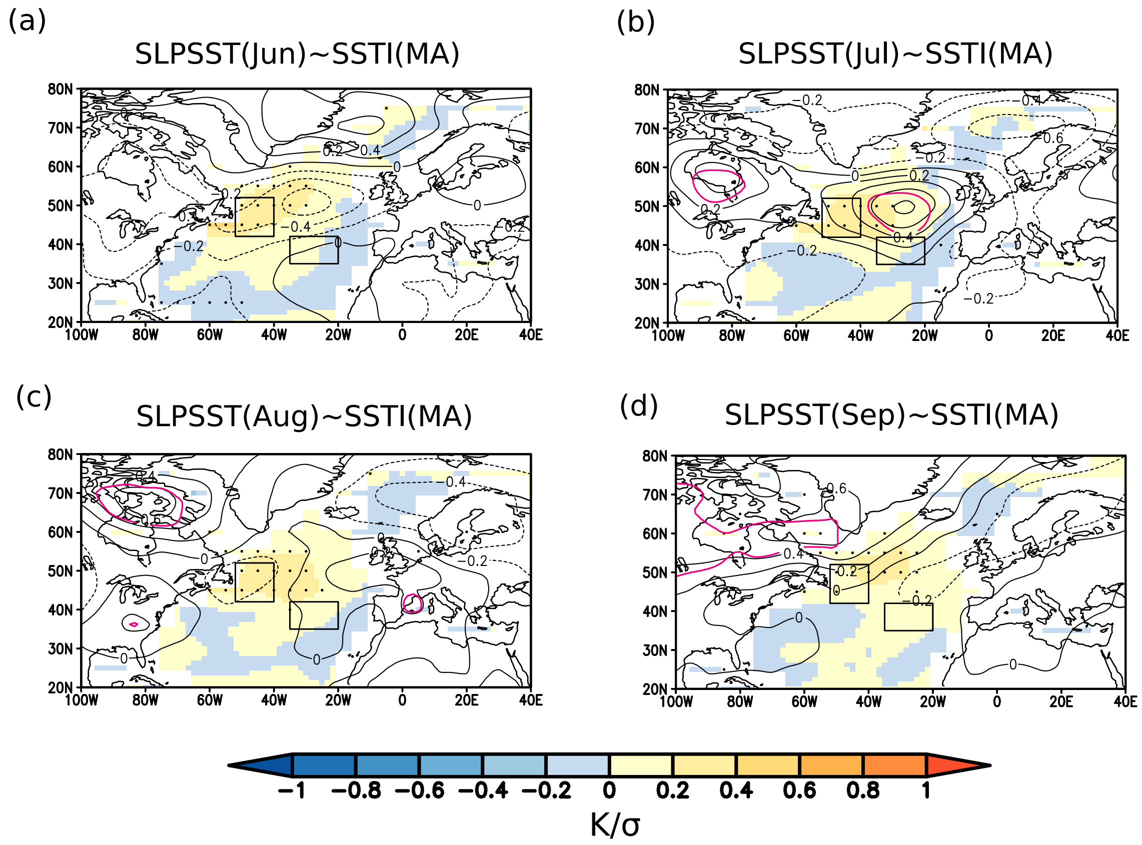

Fig. 9 Same as figure 1 but for 120 years of the GC2 control simulation (See section 2).

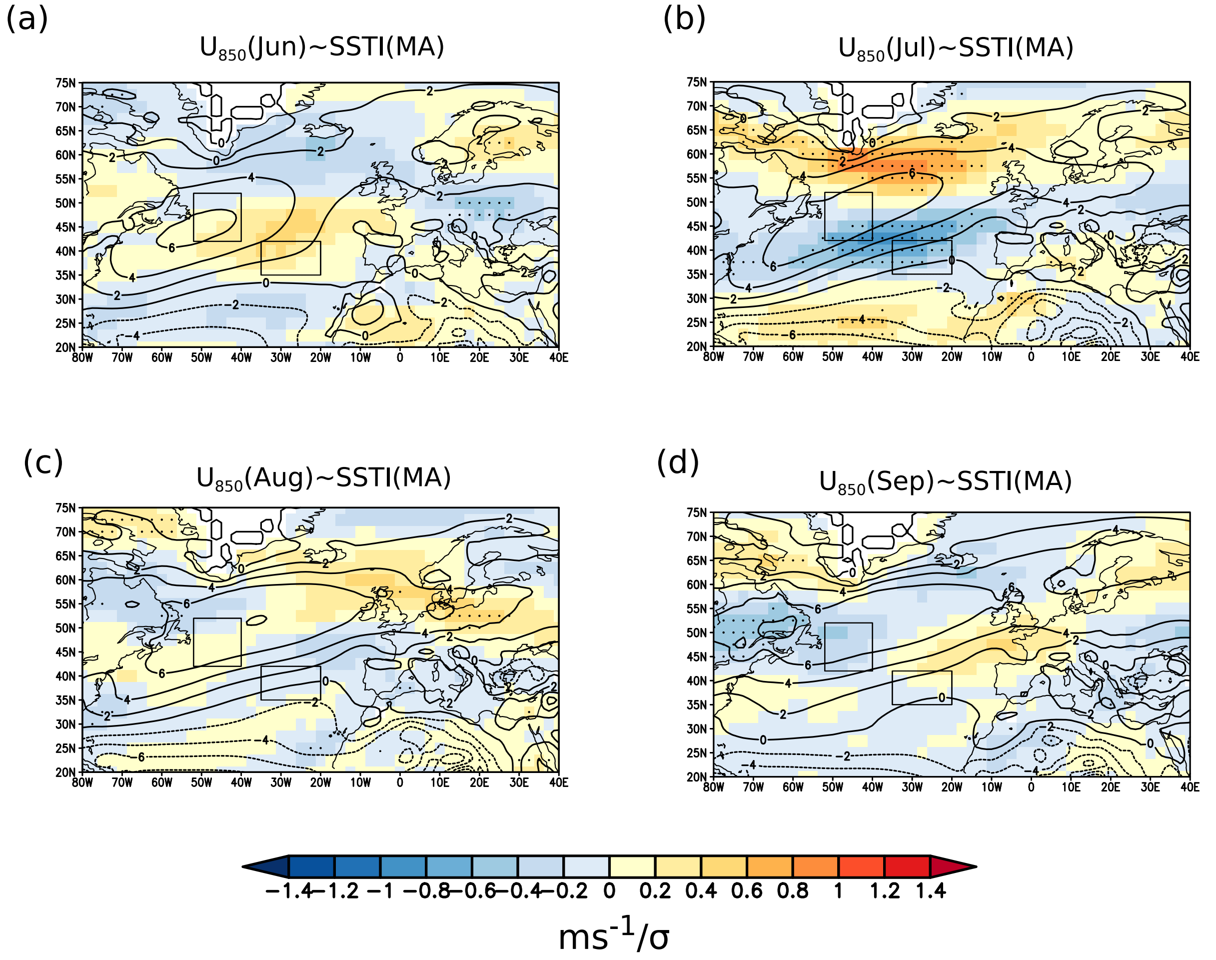

Fig. 10 Same as figure 2a,c,e,g but for 120 years of the GC2 control simulation (See section 2).